

A simple model for internal transport barrier induced by fishbone in tokamak plasmas

Zhaoyang Liu ¹ and Guoyong Fu ^{1,†}

¹Institute for Fusion Theory and Simulation and School of Physics, Zhejiang University, Hangzhou 310027, PR China

(Received 17 July 2023; revised 24 November 2023; accepted 24 November 2023)

Fishbone bursts have been observed to strongly correlate to internal transport barrier (ITB) formation in a number of tokamak devices. A simple model incorporating the fishbone dynamics and ion pressure gradient evolution is proposed in order to investigate the key physics parameters assisting the triggering of ITB. The time evolution of fishbone is described by the well-known predator–prey model. For each burst cycle, the energetic particles (EPs) resonantly interact with fishbone and are radially expelled from inner region leading to a radial current. A compensating bulk plasma return current and, hence, poloidal flow can be induced if the fishbone cycle frequency is greater than the poloidal flow damping rate. When the shear of the poloidal flow exceeds a critical value, the turbulent fluctuations are suppressed and the bulk ion pressure gradient transits to the high-confinement state. It is shown that this process is only sensitive to the deposition rate of the trapped EPs within the $q = 1$ surface, but not sensitive to other parameters. A quantitative formula for the shearing rate of poloidal flow induced by fishbone bursts is derived and verified numerically.

Key words: plasma confinement, plasma dynamics, plasma instabilities

1. Introduction

Since fishbone was observed in the Poloidal Divertor Experiments (PDX) (McGuire *et al.* 1983), it has been widely studied on account of large energetic particle (EP) losses in the presence of such mode (White *et al.* 1983). The fishbone excitation has been explained by the internal kink mode destabilised by trapped EPs as the mode frequency is close to the trapped particle precession frequency (Chen, White & Rosenbluth 1984). A well-known zero-dimensional model, named the predator–prey model (White *et al.* 1983; Chen *et al.* 1984), was proposed to describe the nonlinear instability cycle observed in the experiments (McGuire *et al.* 1983). This model could be derived from the first principle via the nonlinear gyrokinetic equation (Zonca *et al.* 2007), and was recently applied to the estimation of the fishbone cycle frequency quantitatively in tokamak experiments (Xu *et al.* 2015; Zhu *et al.* 2020).

The internal transport barrier (ITB) has been explored in tokamak plasmas in order to improve the core confinement, and to achieve the advanced scenario with high bootstrap current fraction for steady-state operations (Wolf 2003; Connor *et al.* 2004). The physical

† Email address for correspondence: gyfu@zju.edu.cn

mechanisms for the formation and dynamics of the ITB in tokamak and helical plasmas were reviewed in (Ida & Fujita 2018). It is strongly suggested that the key to ITB formation includes radial electric field shear, magnetic shear and rational surface (Ida & Fujita 2018). A theoretical model based on the transport bifurcation has been proposed to predict a power threshold for the transition from low- to high-confinement state locally inside the ITB foot (Diamond *et al.* 1997), and uncover its spatiotemporal dynamics (Newman *et al.* 1998).

Fishbone was first observed to be correlated to ITB formation in ASDEX-Upgrade and the instability was proposed to be responsible for clamping the safety factor q value to the vicinity of unity and avoiding sawteeth (Wolf *et al.* 1999; Gruber *et al.* 2000). During the whistling down period of the fishbone oscillation the transport is reduced around the corresponding rational surface, leading to an increased pressure gradient (Gunter *et al.* 2001). This behaviour could be explained by the redistribution of the resonant EPs resulting in a sheared plasma rotation, which is equivalent to a radial electric field (Pinches *et al.* 2001). Meanwhile, in JET experiments with negative central magnetic shear, the analysis of ITB triggering reveals a correlation between the formation of the ITB and q_{\min} reaching an integer value (Joffrin *et al.* 2002); however, no direct causal relationship to fishbone was reported. In MAST ITB, its onset tends to coincide with the occurrence of the bursts of toroidal Alfvén eigenmodes (TAEs), which are eventually replaced by fishbone instabilities as the q profile decreases, at this time the plasma rotation exhibits a positive gradient just outside q_{\min} surface (Field *et al.* 2011; Clive, Crocker & Hillesheim 2019). In HL-2A tokamak, the flow shear in the stationary ion ITB state reaches the level required for suppressing the ion temperature gradient mode instability, which indicates the important role of flow shear in sustaining the ion ITB (Yu *et al.* 2016). Experimental evidence and simulation analysis suggest that the fishbone activities can induce a poloidal flow, which is beneficial for the suppression of turbulence in the plasma core region (Deng *et al.* 2022). In addition, it has been revealed that fishbone instability is often excited after the ITB formation, and it plays no role in triggering ITB; however, ITBs with fishbone are stronger than without fishbone (He *et al.* 2022). In EAST tokamak, ITB formation is stepwise and always appears after the fishbone instability (Yang *et al.* 2017; Liu *et al.* 2020). It is identified that ITB formation in the ion thermal channel strongly correlates to the excitation of the fishbone (Chu *et al.* 2021; Zhang *et al.* 2022). With neutral beam injection (NBI) power increasing step by step, the magnitude of each burst of fishbone becomes larger and the burst frequency becomes higher and, accordingly, the ITB becomes stronger (Zhu *et al.* 2020; Chu *et al.* 2022). Experimental analysis demonstrates that the increasing $E \times B$ shear flow is important for the formation of ITB (Zhang *et al.* 2023). By using the hybrid kinetic–magnetohydrodynamic (MHD) code M3D-K, single- n simulations showed that when the central gradient of the total pressure profile is above a threshold, the fishbone instability can transport the thermal pressure radially inward and promote the ITB formation (Ren *et al.* 2022). In multiple- n simulations, it is found that a zonal electric field can be induced in the nonlinear fishbone stage, leading to a relatively large $E \times B$ zonal flow that is sufficient for suppressing the dominant micro-instability before ITB formation (Ge *et al.* 2023). A similar process was recently reported in DIII-D plasmas by gyrokinetic and kinetic–MHD simulations; however, it was found that self-generated zonal flows, but not wave–particle interaction, can dominate the fishbone saturation (Brochard *et al.* 2023).

In this paper, a simple model incorporating the fishbone dynamics and ion pressure gradient evolution is proposed in order to investigate the key physics parameters assisting the triggering of ITB. The time evolution of fishbone is described by the well-known predator–prey model (White *et al.* 1983; Chen *et al.* 1984; Zhu *et al.* 2020). For each

burst cycle, the EPs resonantly interact with fishbone and are expelled radially leading to a radial current, and hence a compensating bulk plasma return current. For fishbones that repeat on a timescale faster than the poloidal damping timescale, a sufficient sheared flow driven by plasma current can be induced (Gunter *et al.* 2001; Pinches *et al.* 2001). It should be emphasised that zonal flow generation by fluid nonlinearity is different from the flow driven by plasma current: the former comes from the mode–mode coupling, i.e. Reynolds stress or Maxwell stress, whereas the latter is driven by the $\mathbf{J} \times \mathbf{B}$ torque due to plasma current in the momentum equation. The radial current induced by EP losses during the injection of NBI or alpha particle production has been discussed (Rosenbluth & Hinton 1996; McClements & Thyagaraja 2006; Thyagaraja, Schwander & McClements 2007), which will drive a significant amount of plasma rotation. The temporal evolution of fluctuation level and ion pressure gradient can be described by a simple zero-dimensional model (Diamond *et al.* 1997). When the shear of the flow exceeds a critical value, the turbulent fluctuations are suppressed, and the ion pressure gradient accesses the high-confinement state (Burrell 1997).

The remainder of the paper is organised as follows. The theoretical model is presented in § 2 including a description of fishbone amplitude evolution equation, poloidal rotation driven by radial current and ion transport equation. The corresponding analytical steady-state solutions are derived and verified numerically. Numerical solutions are presented in § 3. Section 4 gives discussions on the simplified model used and the implications of our results for the suppression of turbulence by fishbone. Section 5 gives a summary and conclusions. In Appendix A, the equation for poloidal rotation driven by radial current including neoclassical effects is derived.

2. Theoretical model

2.1. Fishbone amplitude evolution equation

The evolution of EP beta and fishbone amplitude can be described by the well-known predator–prey model (White *et al.* 1983; Chen *et al.* 1984; Zhu *et al.* 2020),

$$\frac{d\beta_{\text{ep}}}{dt} = D - AZ\beta_{\text{max}}H(\beta_{\text{ep}} - \beta_{\text{min}}), \quad (2.1)$$

$$\frac{dA}{dt} = A\Gamma(\beta_{\text{ep}} - \beta_{\text{crit}}), \quad (2.2)$$

where β_{ep} is the average trapped EP beta within the $q = 1$ surface, A is fishbone amplitude ($\equiv \delta B_r/B_0$, the normalised radial perturbed magnetic field), D is the deposition rate of trapped EP within the $q = 1$ surface, Z is a measure of the EP loss rate, $\beta_{\text{max}} = \beta_{\text{crit}}/(1 - f_t/2)$, $\beta_{\text{min}} = (1 - f_t)\beta_{\text{max}} = 2\beta_{\text{crit}} - \beta_{\text{max}}$, f_t is the fraction of trapped EPs that can be ejected, β_{crit} is the excitation threshold of fishbone, Γ is the resonant drive of trapped EPs and H is Heaviside function. The evolution of β_{ep} is periodic with minimum β_{min} and maximum β_{max} . The Hamiltonian of the system (Heidbrink *et al.* 1993), which is conserved and equals the energy C , is given by

$$\mathcal{H}(x, p_x) \equiv \frac{1}{2}\Gamma p_x^2 - Dx + e^x Z \beta_{\text{max}} = C, \quad (2.3)$$

where $x \equiv \ln A$ and $p_x \equiv \beta_{\text{ep}} - \beta_{\text{crit}}$ is the generalised coordinate and momentum, respectively. Equations (2.1) and (2.2) can be derived from (2.3) directly as $\dot{p}_x = -\partial\mathcal{H}/\partial x = D - e^x Z \beta_{\text{max}}$, $\dot{x} = \partial\mathcal{H}/\partial p_x = \Gamma p_x$, where for the steady solution $\beta_{\text{min}} \leq \beta_{\text{ep}} \leq \beta_{\text{max}}$ and $H(\beta_{\text{ep}} - \beta_{\text{min}}) = 1$. From (2.1), one can see that $\beta_{\text{ep}} = \beta_{\text{min}}$ at $A = D/Z\beta_{\text{max}}$,

substituting into (2.3) leads to

$$C = \frac{1}{2} \Gamma (\beta_{\min} - \beta_{\text{crit}})^2 - D \ln \frac{D}{Z\beta_{\max}} + D. \quad (2.4)$$

On the other hand, from (2.2), A is periodic with minimum A_{\min} and maximum A_{\max} at $\beta_{\text{ep}} = \beta_{\text{crit}}$,

$$-D \ln A_{\max} + A_{\max} Z \beta_{\max} = -D \ln A_{\min} + A_{\min} Z \beta_{\max} = C. \quad (2.5)$$

The extrema of A , A_{\min} and A_{\max} can be determined by (2.4) and (2.5). For this reason, there are only five free parameters in the predator–prey model, D , Z , β_{crit} , β_{\max} , Γ .

For Hamilton's equations, the period of fishbone t_p is related to the action $J = \oint p_x dx$ and energy C (Heidbrink *et al.* 1993) by

$$t_p = \frac{dJ}{dC} = \sqrt{\frac{2}{\Gamma}} \int_{A_{\min}}^{A_{\max}} dA \frac{1}{A \sqrt{(A_{\max} - A) Z \beta_{\max} - D \ln(A_{\max}/A)}}. \quad (2.6)$$

The single burst solution can be obtained by expanding around $\beta_{\text{ep}} = \beta_{\text{crit}}$ and $A = A_{\max}$, $\beta_{\text{ep}} \approx \beta_{\text{crit}} + c(t - t_0)$, $\ln A \approx \ln A_{\max} + d(t - t_0)^2/2$, substituting into (2.1) and (2.2), we obtain $c = D - A_{\max} Z \beta_{\max}$, $d = \Gamma c$ and

$$A_s(t) \approx A_{\max} \exp \left[- \left(\frac{t - t_0}{\Delta t} \right)^2 \right], \quad \Delta t = \sqrt{\frac{2}{\Gamma (A_{\max} Z \beta_{\max} - D)}}, \quad (2.7a,b)$$

where t_0 is the time at $A = A_{\max}$. As a result, the solution of successive bursts is constituted as

$$A(t) = \sum_{p=0,1,2,\dots} A_s(t - pt_p) H(t - pt_p) H((p+1)t_p - t). \quad (2.8)$$

This analytical solution has been verified numerically as shown in figure 1, where the red line is the numerical solution of (2.1) and (2.2) and the blue dashed line is the analytical solution of (2.8). The five free parameters are selected as $\beta_{\text{crit}} = 0.001$, $\beta_{\max} = 0.0014$, $\Gamma = 5.0 \times 10^6 \text{ s}^{-1}$, $D = 0.1 \text{ s}^{-1}$ and $Z = 3.0 \times 10^7 \text{ s}^{-1}$, which come from the fitting of EAST experimental data (Xu *et al.* 2015; Zhu *et al.* 2020). The initial conditions are $\beta_{\text{ep}} = \beta_{\text{crit}}$ and $A = A_{\min}$. The maximum A_{\max} in the numerical solution is exactly the same as the value calculated from (2.4) and (2.5). Meanwhile, the burst period t_p and the burst width Δt both coincide with the numerical solution.

2.2. Poloidal rotation driven by EP radial current

It can be shown that (2.1) is essentially the EP transport equation. The flux surface averaged EP charge conservation law is

$$\frac{\partial \rho_{\text{ep}}}{\partial t} + \frac{1}{r} \frac{\partial}{\partial r} (r J_r) = S_{\text{ep}}, \quad (2.9)$$

where $\rho_{\text{ep}} \equiv q_{\text{ep}} n_{\text{ep}}$, q_{ep} and n_{ep} are the EP charge and density, respectively, J_r is the radial current, r is radial coordinate (the simple toroidal coordinate system is adopted and r represents the flux surface) and S_{ep} is the source of EPs. Assuming the radial current

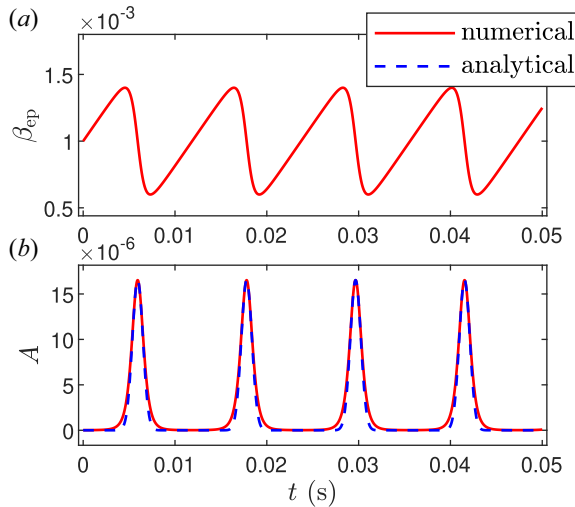


FIGURE 1. Numerical solution (red line) of (2.1) and (2.2), analytical solution (blue dashed line) of (2.8), where the burst period t_p and width Δt are defined in (2.6) and (2.7b), respectively.

comes from interaction of EPs and fishbone, its radial structure can be represented by a Gaussian shape as computed by HAGIS simulations (Pinches *et al.* 2001),

$$J_r(r, t) \approx J(t) \frac{r}{r_0} \exp \left[- \left(\frac{r - r_0}{\Delta r} \right)^2 \right], \tag{2.10}$$

where r_0 is the position of the Gaussian peak which mostly depends on the location in phase space of the dominant precessional resonant response (Fu *et al.* 2006). In practice, $r_0 \sim r_s$ is the position of $q = 1$ surface and $\Delta r \sim r_s$ is the radial width of fishbone. The Gaussian shape used here is just to simplify the model calculation: one can substitute a realistic profile of J_r into simulations or experiments to obtain more precise results. Multiplying by $4\mu_0 T_{ep} r / B_0^2 q_{ep} r_s^2$ and integrating from 0 to r_s in (2.9), we get

$$\frac{d\beta_{ep}}{dt} = D - \frac{4\mu_0 T_{ep}}{B_0^2 q_{ep} r_s} J(t), \tag{2.11}$$

where $\beta_{ep} \equiv 2\mu_0 \bar{n}_{ep} T_{ep} / B_0^2$ is the averaged EP beta, $\bar{n}_{ep} \equiv \int_0^{r_s} 2rn_{ep} dr / r_s^2$ is the averaged EP density, T_{ep} is the EP temperature and is assumed to be a constant, μ_0 is the permeability of vacuum and $D \equiv (4\mu_0 T_{ep} / B_0^2 q_{ep} r_s^2) \int_0^{r_s} S_{ep} r dr$. Comparing with (2.1), one can identify that the radial current is proportional to the fishbone amplitude,

$$J(t) = J_f A(t), J_f \equiv \frac{B_0^2 q_{ep} r_s}{4\mu_0 T_{ep}} Z \beta_{max}. \tag{2.12}$$

There is also a theoretical derivation from the nonlinear gyrokinetic equation (Zonca *et al.* 2007), confirming the linear relation between fishbone amplitude and EP transport flux.

The equation for poloidal rotation driven by radial current (Peeters 1998) is derived in Appendix A as

$$a \frac{\partial V_\theta}{\partial t} = -\nu V_\theta - f J_r, \quad (2.13)$$

where $a = (\epsilon^2/q^2)(1 + 2q^2 + 1.63q^2/\sqrt{\epsilon})$, $1.63q^2/\sqrt{\epsilon}$ comes from the neoclassical effect (Shaing, Ida & Sabbagh 2015), the poloidal flow damping rate $\nu = 1.1\nu_{ii}\sqrt{\epsilon}$ is proportional to the ion-ion collisional frequency ν_{ii} , $f = (\epsilon^2/q^2)(B_0/n_i m_i)$, n_i and m_i are the ion density and mass, respectively, $\epsilon \equiv r/R_0$ and R_0 is major radius of the tokamak. As the radial current $J(t) \propto A(t)$, which is composed of successive bursts, a steady poloidal flow can be built up on condition that the burst frequency is greater than the poloidal flow damping rate. The steady flow for a given radial position can be estimated as follows: here we choose the position of $r = r_s$ for illustration, for other positions near $r = r_s$, the conclusion is qualitatively the same. For $r = r_s$, vanishing of the left-hand side of (2.13) gives the steady solution

$$\langle V_\theta \rangle_t = -\frac{f}{\nu} \langle J_r \rangle_t = -\frac{f}{\nu} J_f \langle A(t) \rangle_t, \quad (2.14)$$

where $\langle \dots \rangle_t$ denotes the long-time average, and is equivalent to the time average over one period, $\langle A(t) \rangle_t = \int_0^{t_p} dt A_s(t)/t_p$. For $\Delta t \leq t_p$, the integral $\int_0^{t_p} dt A_s(t)$ is close to Gaussian integral and $\approx \sqrt{\pi} \Delta t A_{\max}$. As a result, the steady flow can be approximated as

$$\langle V_\theta \rangle_t \approx -\sqrt{\pi} \frac{\Delta t f}{t_p \nu} J_f A_{\max}. \quad (2.15)$$

It can be shown that the steady flow is proportional to $\Delta t/t_p$, which means the larger burst frequency or the longer burst duration would lead to larger steady flow shear and assist in the building of ITB. In order to calculate the radial shear of the poloidal rotation, (2.13) and its radial derivative are written respectively as

$$\frac{\partial V_\theta}{\partial t} = -\frac{\nu}{a} V_\theta - \frac{f}{a} J_r, \quad (2.16)$$

$$\frac{\partial V'_\theta}{\partial t} = -\frac{\nu}{a} V'_\theta - \left(\frac{\nu}{a}\right)' V_\theta - \frac{f}{a} J'_r - \left(\frac{f}{a}\right)' J_r, \quad (2.17)$$

where the prime represents derivative in the radial direction. The flow shear V'_θ can be obtained by solving (2.16) and (2.17) simultaneously. Here we only consider the radial variation of ϵ in the coefficients a , ν and f ; the equilibrium related parameters such as q , ν_{ii} and n_i are assumed to be constant. Since the leading-order term for $\epsilon \ll 1$ in a is $1.63q^2/\sqrt{\epsilon}$, we have $a'/a \approx 3/2r$, $\nu'/\nu = 1/2r$ and $f'/f = 2/r$. The steady flow shear can be estimated by the same method given previously, for $r = r_s$, vanishing of the left-hand side of (2.17) gives

$$\langle V'_\theta \rangle_t \approx -\frac{5\sqrt{\pi}}{2r_s} \frac{\Delta t f}{t_p \nu} J_f A_{\max}. \quad (2.18)$$

Selecting a set of typical tokamak parameters such as $R_0 = 2$ m, $r_s/R_0 = 0.1$, $\nu = 5$ s⁻¹ and $fJ_f = 2.0 \times 10^9$ m s⁻², the numerical solution of (2.16) and (2.17) is displayed in the red line in figure 2(a,b) and the dashed blue line is the analytical steady solution of (2.15) and (2.18), respectively. The poloidal rotation driven by a single burst of (2.7a) is also

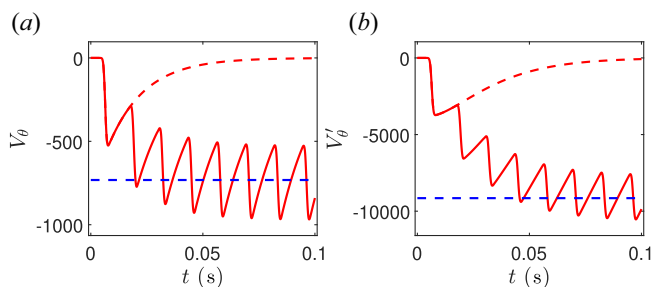


FIGURE 2. (a) Numerical solution (solid red line) of (2.16), where the dashed blue line is the analytical solution of (2.15). (b) Numerical solution (solid red line) of (2.17), where the dashed blue line is the analytical solution of (2.18) and the dashed red line is the poloidal rotation driven by a single burst of (2.7a).

displayed as a dashed red line, and is eventually damped without a steady flow. Note that similar results have been obtained in figure 4 of Pinches *et al.* (2001).

Substituting (2.12) into (2.18) gives an analytical expression to estimate the absolute value of the steady flow shear induced by fishbone bursts,

$$\langle |V'_\theta| \rangle_t \approx \frac{5\sqrt{\pi}}{8.8} \frac{\epsilon^{3/2}}{q^2} \frac{\Omega_{ep}}{v_{ii}} \frac{v_A^2}{v_{ep}^2} \frac{\Delta t}{t_p} Z\beta_{\max} A_{\max}, \quad (2.19)$$

where $v_A \equiv B_0/\sqrt{\mu_0 n_i m_i}$ is the Alfvén velocity, $v_{ep} \equiv \sqrt{T_{ep}/m_{ep}}$ is the EP thermal velocity, $\Omega_{ep} \equiv q_{ep} B_0/m_{ep}$ is the EP gyrofrequency. This quantitative formula can be further simplified when D is small enough, $D \ll A_{\max} Z\beta_{\max}$. By using the relations given by (2.5)–(2.7a,b), the burst width can be approximated as $\Delta t \approx \sqrt{2/(\Gamma A_{\max} Z\beta_{\max})}$, because most of the time $A \ll A_{\max}$, the $AZ\beta_{\max}$ term in the integrand of (2.6) can be neglected; hence, the integral is solved analytically, $t_p \approx 2\sqrt{2A_{\max} Z\beta_{\max}/\Gamma}/D$. As a result, we obtain $\Delta t/t_p \approx D/(2A_{\max} Z\beta_{\max})$ and

$$\langle |V'_\theta| \rangle_t \approx \frac{5\sqrt{\pi}}{17.6} \frac{\epsilon^{3/2}}{q^2} \frac{\Omega_{ep}}{v_{ii}} \frac{v_A^2}{v_{ep}^2} D, \quad (2.20)$$

which means that the steady flow shear grows linearly with D increasing, and it is independent of other parameters of Z , β_{crit} , β_{max} , Γ . This analytical expression is broken as $D \rightarrow A_{\max} Z\beta_{\text{max}}$, since $\Delta t \rightarrow \infty$ as shown in (2.7b). In fact, when $\Delta t > t_p$, the solution of A behaves like oscillation rather than burst; thus, the form of exponential in (2.7a) is incorrect. However, the numerical solution in § 3 still shows the same trend that the steady flow shear only depends on D linearly.

2.3. Ion transport model

The temporal evolution of ion temperature gradient mode (ITG) fluctuation level and ion pressure gradient can be described by a simple zero-dimensional model (Diamond *et al.* 1997; Newman *et al.* 1998),

$$\frac{\partial E}{\partial t} = (\gamma_0 N - \alpha_1 E - \alpha_2 V_E^2) E, \quad (2.21)$$

$$\frac{\partial N}{\partial t} = S - (D_n + D_d E) N, \quad (2.22)$$

where $E \equiv (\tilde{n}/n)^{1/2}$ is the normalised turbulent fluctuation level and $N \equiv (a_0/P_i)(-dP_i/dr)$ is the ion pressure gradient normalised with the minor radius a_0 . The parameter α_1 is determined by the saturation level of the instability in the low-confinement regime and can be estimated by the empirical mix-length model (Diamond *et al.* 1995), $\gamma_0/\alpha_1 \sim \Delta_r/a_0$. The other parameter α_2 is determined from the $E \times B$ shear flow suppression criterion (Biglari, Diamond & Terry 1990; Zhang & Mahajan 1992), $\alpha_2 = (\Delta_r/\Delta_\theta)^2/\gamma_0$. Here, Δ_r and Δ_θ are the turbulent radial and poloidal correlation length, respectively, and assumed to be the same order, $\Delta_r \approx \Delta_\theta$. Here S is the source of thermal ions, and D_n and D_a are the neoclassical and turbulent transport coefficients, respectively. The $E \times B$ flow V_E is determined by the radial ion force balance equation,

$$V_E = V_\theta - \frac{B_\theta}{B} V_\varphi - \frac{1}{eBn_i} \frac{dP_i}{dr}. \quad (2.23)$$

In this paper, we focus on the poloidal rotation induced by fishbone. Neglecting the toroidal rotation V_φ and ion pressure gradient term in (2.23) leads to $V'_E \approx V'_\theta$. As a result, the predator–prey model and the ion transport model are coupled through the sheared poloidal flow term in (2.21).

There are two steady solutions for (2.21) and (2.22): (a) low-confinement solution $(E, N) = (E_L, N_L)$, when the flow shear $V'_\theta \approx 0$, the saturation level of the turbulent fluctuation is $E_L = \gamma_0 N_L/\alpha_1$, and the steady transport satisfies $S = (D_n + D_a E_L) N_L$; and (b) high-confinement solution $(E, N) = (E_H, N_H)$, when the flow shear is larger than a critical value, the turbulent fluctuation is suppressed, $E_H \approx 0$, the transport is neoclassical, $N_H = S/D_n$. The critical value of flow shear is

$$|V'_\theta| \geq V'_{\theta,c} \equiv \gamma_0 \sqrt{S/D_n}. \quad (2.24)$$

3. Numerical results

The simple model incorporating the fishbone dynamics and ion pressure gradient evolution is proposed as (2.1) and (2.2), (2.16) and (2.17), (2.21) and (2.22), and is numerically solved by the Runge–Kutta method provided by the MATLAB ODE45 library. The fishbone- and rotation-related parameters are the same as in §§ 2.1 and 2.2, respectively. The ion-transport-related parameters are selected as $\gamma_0 = 10^4 \text{ s}^{-1}$, $\alpha_1 = 10^5 \text{ s}^{-1}$, $\alpha_2 = 10^{-4} \text{ s}^2$, $S = 10^4 \text{ s}^{-1}$, $D_n = 5.0 \times 10^3 \text{ s}^{-1}$ and $D_a = 2.0 \times 10^5 \text{ s}^{-1}$. The initial turbulent fluctuation level and ion pressure gradient are set as low-confinement solution, $E_L = 0.06$ and $N_L = 0.6$. The corresponding high-confinement solution is $N_H = 2$. In this paper, we focus on the effect of fishbone dynamics on the ITB formation. In other words, five free parameters in the predator–prey model are scanned to investigate which is the key parameter that determines whether the ion pressure gradient can achieve a high-confinement solution, while other parameters are kept fixed.

The temporal evolutions of β_{ep} , A , V'_θ , E and N for $D = 0.10$, $D = 0.12$ and $D = 0.14$ are displayed in figure 3(a). With D increasing, the burst frequency $\sim 1/t_p$, burst width Δt and the maximum of fishbone amplitude A_{\max} all increase. As a result, the steady flow shear V'_θ grows gradually, the turbulent fluctuation E is suppressed and the ion pressure gradient N achieves a high-confinement solution when D exceeds a threshold. The average values of $|V'_\theta|$, E and N over $t = 0.1\text{--}0.2 \text{ s}$ are displayed in figure 3(b). One can see that the transition is stepwise: as D increases from 0.04 to 0.12, the steady flow shear rises gradually to the critical value shown by the dashed grey line, which is given by (2.24). The turbulent fluctuation level reduces to $E_H = 0$ and the ion pressure gradient attains $N_H = 2$ at $D = 0.12$ and remain at these levels even as D grows further. It should be emphasised

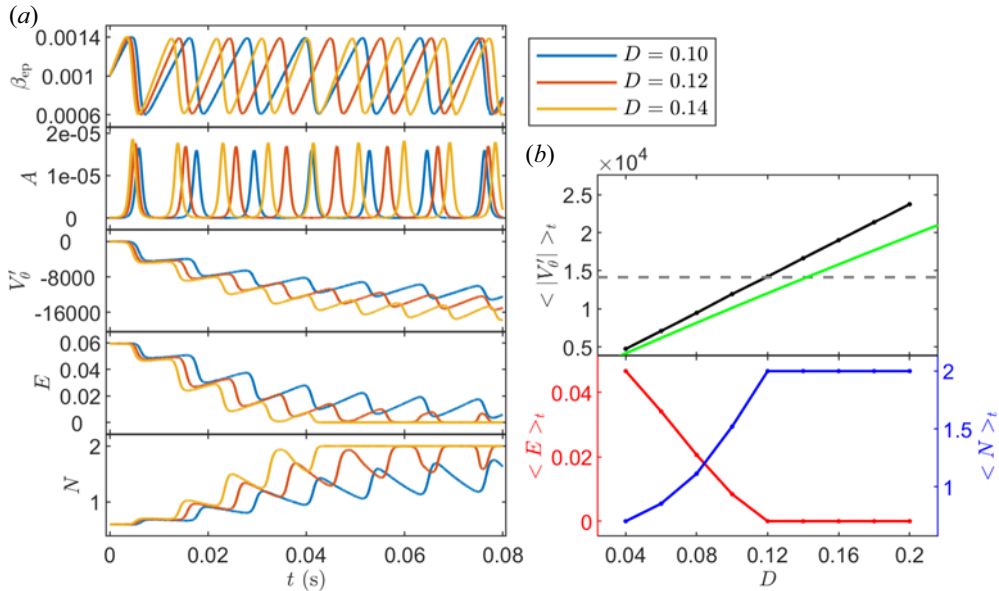


FIGURE 3. (a) Temporal evolutions of β_{ep} , A , V'_θ , E and N for $D = 0.10 \text{ s}^{-1}$, $D = 0.12 \text{ s}^{-1}$ and $D = 0.14 \text{ s}^{-1}$. (b) Average values of $|V'_\theta|$, E and N over $t = 0.1-0.2 \text{ s}$ with D increasing. Other parameters are set as $\beta_{crit} = 0.001$, $\beta_{max} = 0.0014$, $\Gamma = 5.0 \times 10^6 \text{ s}^{-1}$ and $Z = 3.0 \times 10^7 \text{ s}^{-1}$.

that there is a linear relationship between $\langle |V'_\theta| \rangle_t$ and D , and the slope is about 1.2×10^5 , which is a little larger than the analytical solution of the green line given by (2.19).

The temporal evolutions of β_{ep} , A , V'_θ , E and N for $Z = 10^7$, $Z = 3 \times 10^7$ and $Z = 5 \times 10^7$ are displayed in figure 4(a). With Z increasing, the burst frequency $\sim 1/t_p$ and width Δt of A both remain the same; however, only the maximums of A decrease. It can be deduced that AZ is constant from (2.3) and (2.4), hence V'_θ , E and N are unchanged for different Z which is shown in figure 4(a). The average values of $|V'_\theta|$, E and N over $t = 0.1-0.2 \text{ s}$ are displayed in figure 4(b) and are independent of Z .

The temporal evolutions of β_{ep} , A , V'_θ , E and N for $\Gamma = 10^6$, $\Gamma = 5 \times 10^6$ and $\Gamma = 9 \times 10^6$ are displayed in figure 5(a). With Γ increasing, the burst frequency $\sim 1/t_p$ of A increases, and its burst width Δt decreases. As a result, the steady flow shear $\propto (\Delta t/t_p)Z\beta_{max}A_{max}$ remains almost the same, which can be seen in figure 5(b). The average values of E and N over $t = 0.1-0.2 \text{ s}$ show little change.

The temporal evolutions of β_{ep} , A , V'_θ , E and N for $\beta_{max} = 0.0011$, $\beta_{max} = 0.0014$ and $\beta_{max} = 0.0017$ are displayed in figure 6(a). With β_{max} increasing, the burst frequency $\sim 1/t_p$ and width Δt of A both decrease; however, A_{max} increases. As a result, the steady flow shear $\propto (\Delta t/t_p)Z\beta_{max}A_{max}$ remains almost the same, which can be seen in figure 6(b). The average values of E and N over $t = 0.1-0.2 \text{ s}$ also remain almost constant. Similar results for β_{crit} are displayed in figure 7. There is a rapid ramp in the analytical solution of the green line when β_{max} approaches β_{crit} in figures 6(b) and 7(b). The reason is that as $\beta_{max} \rightarrow \beta_{crit}$, $A_{max}Z\beta_{max} \rightarrow D$ and $\Delta t \rightarrow \infty$ in (2.7b), the analytical solution is not valid in this parameter region.

In conclusion, the key parameter that determines the ITB formation is D in fishbone dynamics, whereas other parameters such as Z , β_{crit} , β_{max} and Γ are not significant. The reason is that the long-time average value of the flow shear, even though it oscillates with

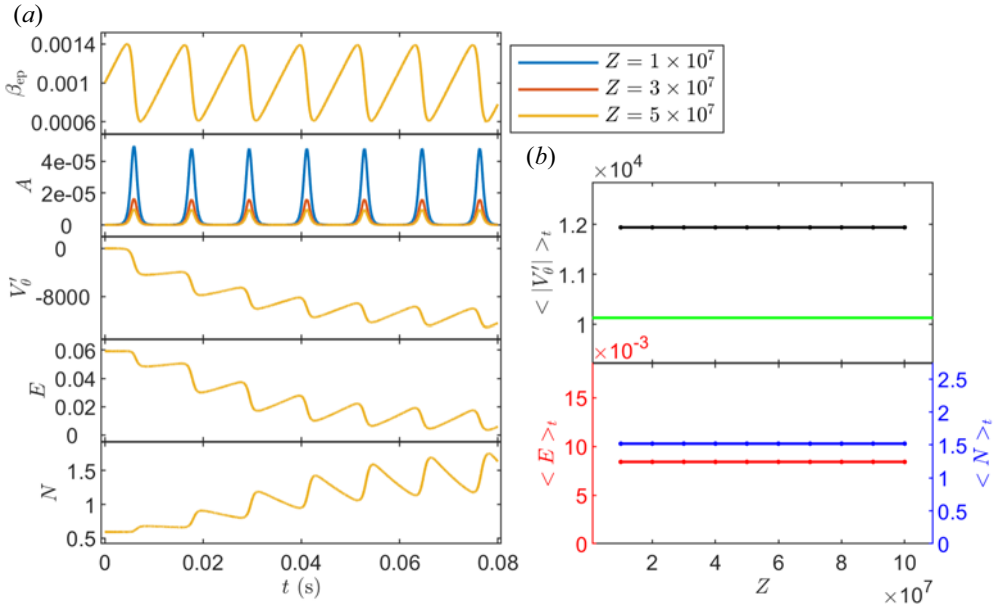


FIGURE 4. (a) Temporal evolutions of β_{ep} , A , V'_θ , E and N for $Z = 10^7 \text{ s}^{-1}$, $Z = 3 \times 10^7 \text{ s}^{-1}$ and $Z = 5 \times 10^7 \text{ s}^{-1}$. (b) Average values of $|V'_\theta|$, E and N over $t = 0.1-0.2 \text{ s}$ with Z increasing. Other parameters are set as $\beta_{crit} = 0.001$, $\beta_{max} = 0.0014$, $\Gamma = 5.0 \times 10^6 \text{ s}^{-1}$ and $D = 1.0 \text{ s}^{-1}$.

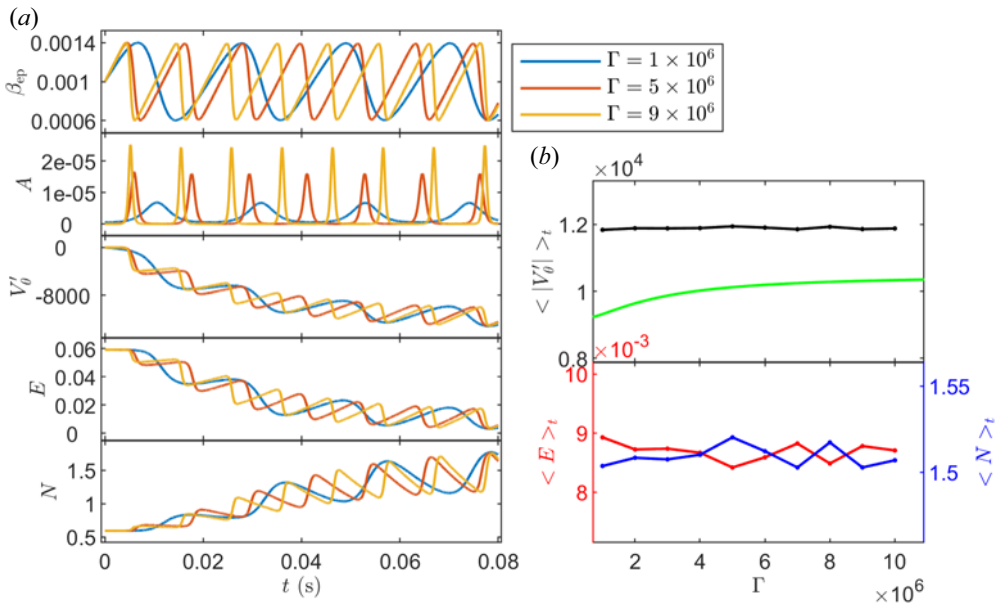


FIGURE 5. (a) Temporal evolutions of β_{ep} , A , V'_θ , E and N for $\Gamma = 10^6 \text{ s}^{-1}$, $\Gamma = 5 \times 10^6 \text{ s}^{-1}$ and $\Gamma = 9 \times 10^6 \text{ s}^{-1}$. (b) Average values of $|V'_\theta|$, E and N over $t = 0.1-0.2 \text{ s}$ with Γ increasing. Other parameters are set as $\beta_{crit} = 0.001$, $\beta_{max} = 0.0014$, $D = 0.1 \text{ s}^{-1}$ and $Z = 3.0 \times 10^7 \text{ s}^{-1}$.

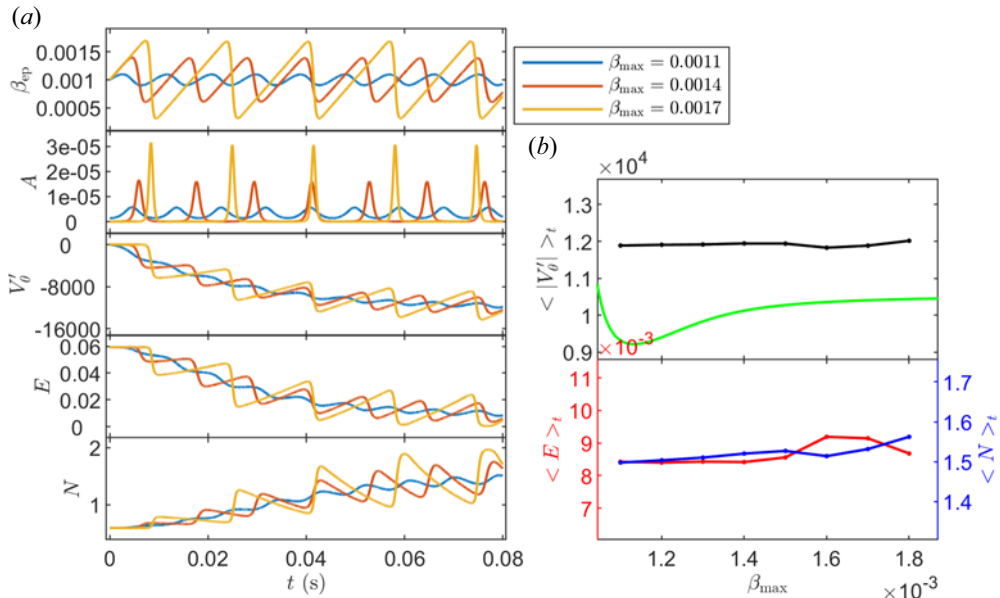


FIGURE 6. (a) Temporal evolutions of β_{ep} , A , V'_θ , E and N for $\beta_{max} = 0.0011$, $\beta_{max} = 0.0014$ and $\beta_{max} = 0.0017$. (b) Average values of $|V'_\theta|$, E and N over $t = 0.1-0.2$ s with β_{max} increasing. Other parameters are set as $\beta_{crit} = 0.001$, $\Gamma = 5.0 \times 10^6 \text{ s}^{-1}$, $D = 0.1 \text{ s}^{-1}$ and $Z = 3.0 \times 10^7 \text{ s}^{-1}$.

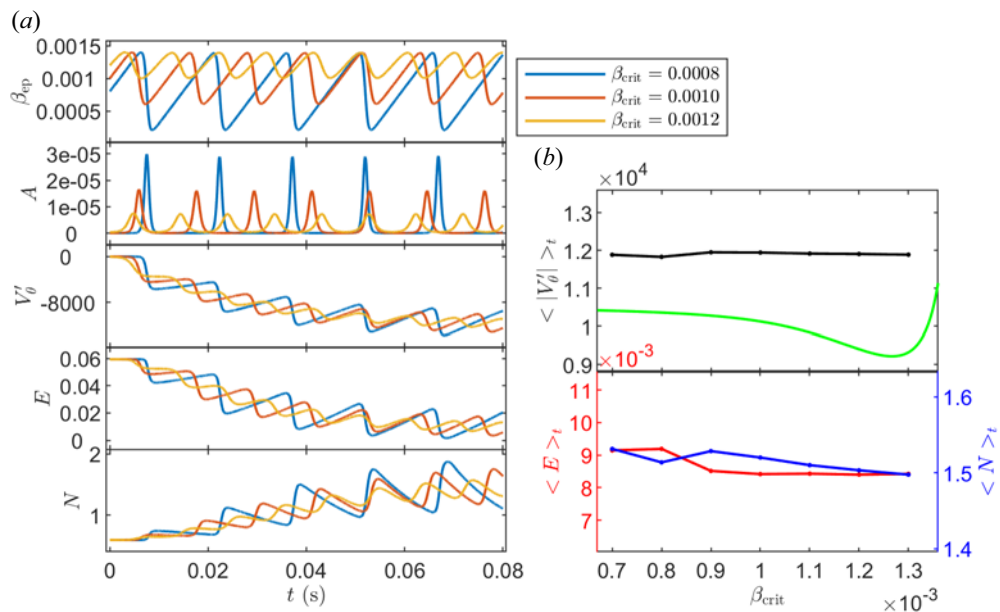


FIGURE 7. (a) Temporal evolutions of β_{ep} , A , V'_θ , E and N for $\beta_{crit} = 0.0008$, $\beta_{crit} = 0.001$ and $\beta_{crit} = 0.0012$. (b) Average values of $|V'_\theta|$, E and N over $t = 0.1-0.2$ s with β_{crit} increasing. Other parameters are set as $\beta_{max} = 0.0014$, $\Gamma = 5.0 \times 10^6 \text{ s}^{-1}$, $D = 0.1 \text{ s}^{-1}$ and $Z = 3.0 \times 10^7 \text{ s}^{-1}$.

different amplitudes, grows linearly with increasing D ; however, it remains almost constant when varying other parameters. Upon the steady flow shear exceeding the critical value of low- to high-confinement transition, the turbulent fluctuation level reduces to zero and the ion pressure gradient attains high-confinement solution leading to the ITB formation around the $q = 1$ surface.

4. Discussion

Before presenting our summary and conclusions, we discuss the simplified models adopted in this paper and the implications of our results on the suppression of micro-turbulence by fishbone.

Regarding the predator–prey model, in order to derive the zero-dimensional predator–prey model from one-dimensional equations, the dynamics due to time-dependent frequency shifts is neglected. It is assumed that β_{ep} can be described by a characteristic spatial scale $\Delta \lesssim r_s$ and $\partial_r \sim 1/\Delta$, $\partial_r^2 \sim -1/\Delta^2$ (Zonca *et al.* 2007). Furthermore, in the EP transport equation (2.1), the diffusive transport is neglected by the assumption that it is much smaller than the convective transport originated from fishbone. The physics of EPs slowing down is also neglected in this model. If we keep this term, (2.1) could be written as

$$\frac{d\beta_{\text{ep}}}{dt} = D - AZ\beta_{\text{max}}H(\beta_{\text{ep}} - \beta_{\text{min}}) - \frac{\beta_{\text{ep}}}{\tau_s}, \quad (4.1)$$

where τ_s represents the EP slowing-down time. Note that there is an equilibrium solution $\beta_{\text{ep}} = D\tau_s$ at $A = 0$, fishbone is unstable for $\beta_{\text{ep}} > \beta_{\text{crit}}$, which indicates that τ_s cannot be too small. Selecting a set of typical tokamak parameters such as $n_i \approx 2.5 \times 10^{19} \text{ m}^{-3}$, $T_i \approx 1 \text{ keV}$, the ion–ion collision time $\tau_i \approx 0.002 \text{ s}$ and $\tau_s \approx (\tau_i/2\sqrt{2})\sqrt{m_i/m_e} \approx 0.03 \text{ s}$ (here $m_{\text{ep}} \approx m_i$ is used), which is larger than fishbone burst period $t_p \approx 0.0119 \text{ s}$ in figure 1. In order to investigate the effect of τ_s , the numerical solution of the predator–prey model and poloidal flow shear with different τ_s is displayed in figure 8, other parameters are the same as in figures 1 and 2. One can see that for $\tau_s < t_p$, β_{ep} remains its initial value and there is no fishbone instability. As for $\tau_s > t_p$, β_{ep} behaves like a dying oscillation, in each successive period, β_{max} and A_{max} decreases continuously. According to formula (2.20), Δt increases and t_p decreases, which coincides with the results in figure 8. Comparing with the results without τ_s term, the numerical solution remains qualitatively unchanged when $\tau_s \gg t_p$.

For the ion transport model, it is a semi-empirical model in which the coefficients γ_0 , α_1 , α_2 , D_n and D_a should be functions of radius and related to a lot of factors, nevertheless, they are all simply taken as constants. It only provides a qualitative description of the transport dynamics (Diamond *et al.* 1997), and more complete transport model is necessary to explore the transport transition and threshold effects (Newman *et al.* 1998). Furthermore, in this work, we focus on the poloidal rotation induced by fishbone, and we assume that the toroidal rotation term and the ion pressure gradient term can be neglected before ITB forms. According to the radial ion force balance (2.23), the conditions for $V'_E \approx V'_\theta$ are $|V'_\theta| > |(V_\varphi B_\theta/B)'$ and $|V'_\theta| > |V'_{*i}|$, where $V_{*i} \equiv (1/eBn_i)(dP_i/dr)$ is the ion diamagnetic velocity.

Finally, we discuss the implication of our results for suppression of micro-turbulence by fishbone. A figure of merit for fishbone stabilisation of turbulence can be derived as follows. The condition for suppression of ITG turbulence is $|V'_\theta| > \gamma_{\text{ITG}}$, where the ITG growth rate $\gamma_{\text{ITG}} \propto V_i/L_{P_i}$, $V_i \equiv \sqrt{T_i/m_i}$ is the ion thermal velocity, $L_{P_i} \equiv -P_i/(dP_i/dr)$

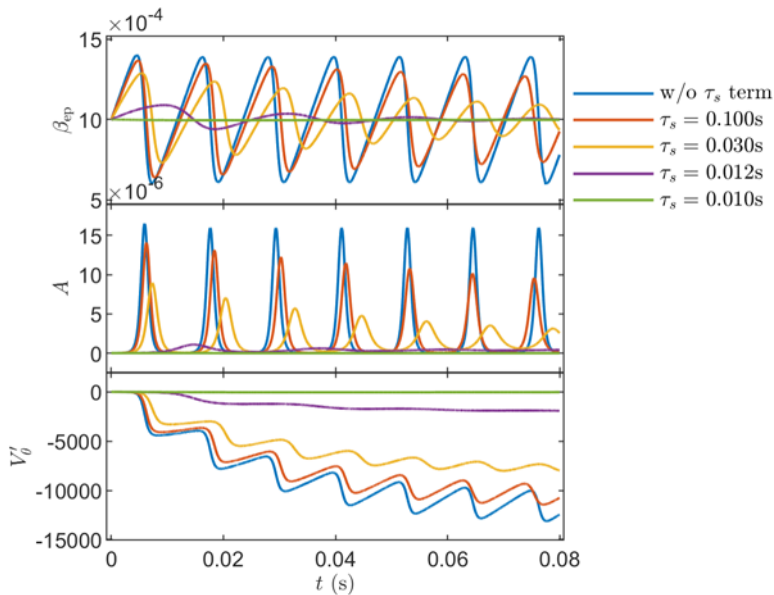


FIGURE 8. Numerical solution of the predator–prey model and poloidal flow shear with different τ_s ; other parameters are the same as in figures 1 and 2.

is the scale length of thermal ion pressure profile. Substituting into (2.20) gives

$$\frac{|V'_\theta|}{\gamma_{\text{ITG}}} \propto \frac{\epsilon^{3/2} \bar{n}_{\text{ep}} L_{P_i}}{q^2 n_i \rho_i}, \quad (4.2)$$

where \bar{n}_{ep} is equilibrium EP density, $\bar{\beta}_{\text{ep}} = D\tau_s$ has been used and $v_{ii}\tau_s$ is a constant. Therefore, we can define a figure of merit Q_{fishbone} for suppression of ITG turbulence as follows:

$$Q_{\text{fishbone}} = \frac{\epsilon^{3/2} \bar{n}_{\text{ep}} L_{P_i}}{q^2 n_i \rho_i}. \quad (4.3)$$

This result indicates that suppression of ITG turbulence and formation of ITB is more likely for larger values of Q_{fishbone} .

5. Summary and conclusions

In this paper, fishbone dynamics is described by the well-known predator–prey model (White *et al.* 1983; Chen *et al.* 1984; Zhu *et al.* 2020), (2.1) and (2.2). It is shown that there are only five free parameters in this model, D , Z , β_{crit} , β_{max} and Γ . The evolution of EP beta β_{ep} is bounded between β_{min} and β_{max} , and the minimum and maximum of fishbone amplitude A can be determined by (2.4) and (2.5). The fishbone induces redistribution of resonant EPs, and the EPs' convective transport leads to a radial current, which is proportional to the fishbone amplitude (Zonca *et al.* 2007). In order to satisfy the quasi-neutral condition, there must be a compensating plasma current with the same value and opposite direction. This radial current can drive plasma poloidal rotation through the $\mathbf{J} \times \mathbf{B}$ torque (Rosenbluth & Hinton 1996; Peeters 1998; McClements & Thyagaraja 2006; Thyagaraja *et al.* 2007), which is given in (2.13) and deduced in Appendix A, including the neoclassical effects (Shaing *et al.* 2015). Because the fishbone amplitude constitutes successive bursts, steady poloidal flow can only be built up on condition that

the burst frequency is greater than the poloidal flow damping rate (Pinches *et al.* 2001). The absolute value of the steady flow shear can be analytically estimated by (2.19), and further simplified by (2.20) for small D (the deposition rate of trapped EPs within the $q = 1$ surface). The result indicates that the steady flow shear grows linearly with D increasing, and remains almost unchanged when varying other parameters of Z , β_{crit} , β_{max} and Γ , which has been numerically verified in § 3. Upon the flow shear exceeding the critical value given by (2.22), the turbulent fluctuation level reduces to zero and the ion pressure gradient attains the high-confinement state, assisting ITB formation. The transition process shown in figure 3 is stepwise, which coincides with the EAST experiments (Yang *et al.* 2017; Chu *et al.* 2022). Note that in Chu *et al.* (2022), the experimental results showed that the higher NBI heating power leads to the stronger ITB. A figure of merit, Q_{fishbone} given in above equation, has been derived based on (2.20). The suppression of ITG turbulence and formation of ITB by fishbone is more likely for larger values of Q_{fishbone} .

This conclusion is qualitative, since it is derived from the simple zero-dimensional model. Extension to a one-dimensional model to obtain more quantitative results and uncover the spatiotemporal dynamics of the transition is left as future work. The radial distribution of the radial current should also be calculated more self-consistently by numerical simulations, for example, via M3D-K code (Fu *et al.* 2006). The $E \times B$ shear considered in this paper comes from the poloidal rotation driven by the radial current induced by fishbone: the effect of toroidal rotation and ion pressure gradient is beyond the scope of this paper. Considering the effect of the ion pressure gradient's contribution to the $E \times B$ shear would lead to a more interesting transport bifurcation process (Diamond *et al.* 1997).

Acknowledgements

We thank Dr F. Zonca for useful discussions related to the fishbone dynamic model.

Editor P. Helander thanks the referees for their advice in evaluating this article.

Funding

This work is supported by the National MCF Energy R&D Program of China (Grant No. 2019YFE03050001).

Declaration of interests

The authors report no conflict of interest.

Appendix A. Equation for poloidal rotation driven by radial current including neoclassical effect

The plasma flow evolution equation can be obtained by summing the electron and ion momentum equations as (Rosenbluth & Hinton 1996; Peeters 1998)

$$n_i m_i \frac{\partial V}{\partial t} = J_p \times B - \nabla P - \nabla \cdot \pi, \quad (\text{A1})$$

where V is plasma flow, J_p is plasma current and P and π are the pressure scalar and tensor, respectively. The projection of (A1) on the direction of magnetic field and torus

respectively are

$$n_i m_i \frac{\partial}{\partial t} (\mathbf{B} \cdot \mathbf{V}) = -\mathbf{B} \cdot \nabla P - \mathbf{B} \cdot \nabla \cdot \boldsymbol{\pi}, \tag{A2}$$

$$n_i m_i \frac{\partial}{\partial t} (R \mathbf{e}_t \cdot \mathbf{V}) = R \mathbf{e}_t \cdot \mathbf{J}_p \times \mathbf{B} - R \mathbf{e}_t \cdot \nabla P - R \mathbf{e}_t \cdot \nabla \cdot \boldsymbol{\pi}. \tag{A3}$$

After averaging over magnetic surface, one obtains

$$n_i m_i \frac{\partial}{\partial t} \langle B V_{\parallel} \rangle = -\langle \mathbf{B} \cdot \nabla \cdot \boldsymbol{\pi} \rangle, \tag{A4}$$

$$n_i m_i \frac{\partial}{\partial t} \langle R V_t \rangle = -\langle R B_p J_p^r \rangle, \tag{A5}$$

where we have defined $\mathbf{B} = B_t \mathbf{e}_t + B_p \mathbf{e}_p$, the subscripts t and p representing toroidal and poloidal, respectively, and the coordinate is right-hand, $\mathbf{e}_r \equiv \mathbf{e}_t \times \mathbf{e}_p$. The magnetic surface average is defined as $\langle G \rangle \equiv \oint ds G/B / \oint ds/B$ and $\langle \mathbf{B} \cdot \nabla P \rangle = 0$, $R \mathbf{e}_t \cdot \nabla P + R \mathbf{e}_t \cdot \nabla \cdot \boldsymbol{\pi} = 0$ because of toroidal symmetry.

The plasma flow perpendicular to the magnetic field in lowest order is (Peeters 1998)

$$\mathbf{V}_{\perp} = \frac{E^{*r}}{B^2} (B_t \mathbf{e}_p - B_p \mathbf{e}_t), \tag{A6}$$

where $E^{*r} \equiv E^* \cdot \nabla r$ and $E^* = -\nabla \phi - \nabla P_i / n_i e$ is the effective electric field. As the plasma flow is less than the sound velocity, it is incompressible and can be expressed as $\mathbf{V} = K(\psi_p) \mathbf{B} + G(\psi_p) R \mathbf{e}_t$, where $K(\psi_p)$ and $G(\psi_p)$ are flux functions,

$$K(\psi_p) = \langle V_p \rangle / \langle B_p \rangle, G(\psi_p) = -\langle E^{*r} \rangle / \langle R B_p \rangle. \tag{A7}$$

Substituting (A7) into (A4) and (A5), one obtains

$$n_i m_i \frac{\langle B^2 \rangle}{\langle B_p \rangle} \frac{\partial}{\partial t} \langle V_p \rangle - n_i m_i \frac{\langle R B_t \rangle}{\langle R B_p \rangle} \frac{\partial}{\partial t} \langle E^{*r} \rangle = -\langle \mathbf{B} \cdot \nabla \cdot \boldsymbol{\pi} \rangle, \tag{A8}$$

$$n_i m_i \frac{\langle R B_t \rangle}{\langle B_p \rangle} \frac{\partial}{\partial t} \langle V_p \rangle - n_i m_i \frac{\langle R^2 \rangle}{\langle R B_p \rangle} \frac{\partial}{\partial t} \langle E^{*r} \rangle = -\langle R B_p J_p^r \rangle. \tag{A9}$$

The plasma current is determined as follows (Rosenbluth & Hinton 1996): when there is radial current due to the interaction of EPs and fishbone, the plasma must carry a compensating current to satisfy the quasi-neutral condition, $\langle R B_p J_p^r \rangle = -\langle J^{\psi_p} \rangle$. Including the neoclassical effect (Shaing *et al.* 2015),

$$\langle \mathbf{B} \cdot \nabla \cdot \boldsymbol{\pi} \rangle \approx n_i m_i \frac{\langle B^2 \rangle}{\langle B_p \rangle} \left(1.1 v_{ii} \sqrt{\epsilon} \langle V_p \rangle + 1.63 \epsilon^{3/2} \frac{\partial \langle V_p \rangle}{\partial t} \right). \tag{A10}$$

By eliminating $\langle E^{*r} \rangle$ in (A8) and (A9), and using the lowest-order equilibrium $R = R_0(1 + \epsilon \cos \theta)$, the magnetic surface average is $\langle G \rangle = \oint d\theta (1 + \epsilon \cos \theta) G$, and the equation for

poloidal rotation $V_\theta \equiv \langle V_p \rangle$ is

$$\frac{\epsilon^2}{q^2} \left(1 + 2q^2 + 1.63 \frac{q^2}{\sqrt{\epsilon}} \right) \frac{\partial V_\theta}{\partial t} = -1.1 v_{ii} \sqrt{\epsilon} V_\theta - \frac{\epsilon}{n_i m_i R_0 q} \left[1 - \frac{\epsilon^2}{q^2} (1 + 2q^2) \right] \langle J^{\psi_p} \rangle. \quad (\text{A11})$$

In (A11), $\langle J^{\psi_p} \rangle = |\nabla \psi_p| J_r$ is the contravariant component of current induced by fishbone. A similar equation for poloidal rotation has been derived in Peeters (1998) and Shaing *et al.* (2015); here, use is made of the lowest-order equilibrium to express the coefficients as function of ϵ .

REFERENCES

- BIGLARI, H., DIAMOND, P.H. & TERRY, P.W. 1990 Influence of sheared poloidal rotation on edge turbulence. *Phys. Fluids B* **2** (1), 1–4.
- BROCHARD, G., LIU, C., WEI, X., HEIDBRINK, W., LIN, Z., GORELENKOV, N., CHRYSTAL, C., DU, X., BAO, J., POLEVOI, A.R., *et al.* 2023 Saturation of fishbone instability by self-generated zonal flows in tokamak plasmas. arXiv:2301.01792. Accepted by *Phys. Rev. Lett.* on 9 November 2023.
- BURRELL, K.H. 1997 Effects of $E \times B$ velocity shear and magnetic shear on turbulence and transport in magnetic confinement devices. *Phys. Plasmas* **4** (5, 2), 1499–1518, 38th Annual Meeting of the Division of Plasma Physics of the American Physical Society, Denver, CO, Nov, 11–15, 1996.
- CHEN, L., WHITE, R.B. & ROSENBLUTH, M.N. 1984 Excitation of internal kink modes by trapped energetic beam ions. *Phys. Rev. Lett.* **52** (13), 1122–1125.
- CHU, Y.Q., LIU, H.Q., ZHANG, S.B., JIE, Y.X., LIAN, H., WU, M.Q., ZHU, X., WU, C.B., XU, L.Q., WANG, Y.F., *et al.* 2021 Study of the mechanism of ITB formation and sustainment with optimized q profiles in ELMy H mode discharges on the EAST. *Plasma Phys. Control. Fusion* **63**, 105003.
- CHU, Y., LIU, H., ZHANG, S., XU, L., LI, E., JIE, Y., LIAN, H., ZHOU, T., FENG, X., ZHANG, X., *et al.* 2022 Magneto-hydrodynamic effect of internal transport barrier on EAST tokamak. *Plasma Sci. Technol.* **24**, 035102.
- CLIVE, M., CROCKER, N. & HILLESHEIM, J. 2019 Influence of fishbone-induced fast-ion losses on rotation and transport barrier formation in MAST. In 16th IAEA Technical Meeting on Energetic Particles in Magnetic Confinement Systems - Theory of Plasma Instabilities.
- CONNOR, J.W., FUKUDA, T., GARBET, X., GORMEZANO, C., MUKHOVATOV, V., WAKATANI, M., ITB DATABASE GRP & ITPA TOPICAL GRP TRANSPORT INTERN 2004 A review of internal transport barrier physics for steady-state operation of tokamaks. *Nucl. Fusion* **44** (4), R1–R49.
- DENG, W., LIU, Y., GE, W.L., JIANG, M., SHI, Z.B., LI, D., JI, X.Q., DONG, Y.B., WANG, F., CAO, J.Y., *et al.* 2022 Investigation of the role of fishbone activity in the formation of internal transport barrier in HL-2A plasma. *Phys. Plasmas* **29**, 102106.
- DIAMOND, P.H., LEBEDEV, V.B., NEWMAN, D.E. & CARRERAS, B.A. 1995 Dynamics of spatiotemporally propagating transport barriers. *Phys. Plasmas* **2** (10), 3685–3695.
- DIAMOND, P.H., LEBEDEV, V.B., NEWMAN, D.E., CARRERAS, B.A., HAHM, T.S., TANG, W.M., REWOLDT, G. & AVINASH, K. 1997 Dynamics of transition to enhanced confinement in reversed magnetic shear discharges. *Phys. Rev. Lett.* **78** (8), 1472–1475.
- FIELD, A.R., MICHAEL, C., AKERS, R.J., CANDY, J., COLYER, G., GUTTENFELDER, W., GHIM, Y.C., ROACH, C.M., SAARELMA, S. & MAST TEAM 2011 Plasma rotation and transport in MAST spherical tokamak. *Nucl. Fusion* **51**, 063006.
- FU, G.Y., PARK, W., STRAUSS, H.R., BRESLAU, J., CHEN, J., JARDIN, S. & SUGIYAMA, L.E. 2006 Global hybrid simulations of energetic particle effects on the $n = 1$ mode in tokamaks: internal kink and fishbone instability. *Phys. Plasmas* **13**, 052517.
- GE, W., WANG, Z.-X., WANG, F., LIU, Z. & XU, L. 2023 Multiple interactions between fishbone instabilities and internal transport barriers in EAST plasmas. *Nucl. Fusion* **63**, 016007.
- GRUBER, O., WOLF, R., BOSCH, H.S., DUX, R., GUNTHER, S., MCCARTHY, P.J., LACKNER, K., MARASCHEK, M., MEISTER, H., PEREVERZEV, G., *et al.* 2000 Steady state H mode and $T_e \approx T_i$

- operation with internal transport barriers in ASDEX upgrade. *Nucl. Fusion* **40** (6), 1145–1155, 2nd IAEA Technical Committee Meeting on Steady State Operation of Magnetic Fusion Devices, Plasma Control and Plasma Facing Components, Fukuoka, Japan, Oct 25–29, 1999.
- GUNTER, S., GUDE, A., HOBIRK, J., MARASCHEK, M., SAARELMA, S., SCHADE, S., WOLF, R.C. & ASDEX UPGRADE TEAM 2001 MHD phenomena in advanced scenarios on ASDEX upgrade and the influence of localized electron heating and current drive. *Nucl. Fusion* **41** (9), 1283–1290.
- HE, X.X., YAN, L.W., YU, D.L., CHEN, W., YU, L.M., MA, Q., LIU, L., WEI, Y.L., HE, X.F., ZHANG, N., *et al.* 2022 The ITB dynamics controlled by internal kink modes on HL-2A tokamak. *Plasma Phys. Control. Fusion* **64**, 015007.
- HEIDBRINK, W.W., DUONG, H.H., MANSON, J., WILFRID, E., OBERMAN, C. & STRAIT, E.J. 1993 The nonlinear saturation of beam-driven instabilities – theory and experiment. *Phys. Fluids B* **5** (7, 1), 2176–2186.
- IDA, K. & FUJITA, T. 2018 Internal transport barrier in tokamak and helical plasmas. *Plasma Phys. Control. Fusion* **60**, 033001.
- JOFFRIN, E., GORINI, G., CHALLIS, C.D., HAWKES, N.C., HENDER, T.C., HOWELL, D.F., MAGET, P., MANTICA, P., MAZON, D., SHARAPOV, S.E., *et al.* 2002 Triggering of internal transport barrier in jet. *Plasma Phys. Control. Fusion* **44** (8), 1739–1752.
- LIU, Z.X., GE, W.L., WANG, F., LIU, Y.J., YANG, Y., WU, M.Q., WANG, Z.X., ZHANG, X.X., LI, H., XIE, J.L., *et al.* 2020 Experimental observation and simulation analysis of the relationship between the fishbone and ITB formation on EAST tokamak. *Nucl. Fusion* **60**, 122001.
- MCCLEMENTS, K.G. & THYAGARAJA, A. 2006 Collective electric field effects on the confinement of fast ions in tokamaks. *Phys. Plasmas* **13**, 042503.
- MCGUIRE, K., GOLDSTON, R., BELL, M., BITTER, M., BOL, K., BRAU, K., BUCHENAUER, D., CROWLEY, T., DAVIS, S., DYLLA, F., *et al.* 1983 Study of high-beta magnetohydrodynamic modes and fast-ion losses in PDX. *Phys. Rev. Lett.* **50** (12), 891–895.
- NEWMAN, D.E., CARRERAS, B.A., LOPEZ-BRUNA, D., DIAMOND, P.H. & LEBEDEV, V.B. 1998 Dynamics and control of internal transport barriers in reversed shear discharges. *Phys. Plasmas* **5** (4), 938–952.
- PEETERS, A.G. 1998 Equations for the evolution of the radial electric field and poloidal rotation in toroidally symmetric geometry. *Phys. Plasmas* **5** (3), 763–767.
- PINCHES, S.D., GÜNTER, S., PEETERS, A.G., THE ASDEX UPGRADE TEAM 2001 Fishbone generation of sheared flows in the creation of transport barriers. In *28th EPS Conference on Controlled Fusion and Plasma Physics*, pp. 57–60.
- REN, Z., SHEN, W., LI, G., WU, M., YANG, J. & WANG, W. 2022 Numerical investigation of the fishbone instability effect on thermal pressure in EAST tokamak. *AIP Adv.* **12**, 075318.
- ROSENBLUTH, M.N. & HINTON, F.L. 1996 Plasma rotation driven by alpha particles in a tokamak reactor. *Nucl. Fusion* **36** (1), 55–67.
- SHAING, K.C., IDA, K. & SABBAGH, S.A. 2015 Neoclassical plasma viscosity and transport processes in non-axisymmetric tori. *Nucl. Fusion* **55** (12), 125001.
- THYAGARAJA, A., SCHWANDER, F. & MCCLEMENTS, K.G. 2007 Rotation driven by fast ions in tokamaks. *Phys. Plasmas* **14** (11), 112504.
- WHITE, R.B., GOLDSTON, R.J., MCGUIRE, K., BOOZER, A.H., MONTICELLO, D.A. & PARK, W. 1983 Theory of mode-induced beam particle loss in tokamaks. *Phys. Fluids* **26** (10), 2958–2965.
- WOLF, R.C. 2003 Internal transport barriers in tokamak plasmas. *Plasma Phys. Control. Fusion* **45** (1), R1–R91.
- WOLF, R.C., GRUBER, O., MARASCHEK, M., DUX, R., FUCHS, C., GUNTER, S., HERRMANN, A., KALLENBACH, A., LACKNER, K., MCCARTHY, P.J., *et al.* 1999 Stationary advanced scenarios with internal transport barrier on ASDEX upgrade. *Plasma Phys. Control. Fusion* **41** (12B), B93–B107, 26th European-Physical-Society Conference on Controlled Fusion and Plasma Physics, Maastricht, Netherlands, Jun 14–18, 1999.
- XU, L., ZHANG, J., CHEN, K., HU, L., LI, E., LIN, S., SHI, T., DUAN, Y. & ZHU, Y. 2015 Fishbone activity in experimental advanced superconducting tokamak neutral beam injection plasma. *Phys. Plasmas* **22** (12), 122510.

- YANG, Y., GAO, X., LIU, H.Q., LI, G.Q., ZHANG, T., ZENG, L., LIU, Y.K., WU, M.Q., KONG, D.F., MING, T.F., *et al.* 2017 Observation of internal transport barrier in ELMy H-mode plasmas on the EAST tokamak. *Plasma Phys. Control. Fusion* **59** (8), 085003.
- YU, D.L., WEI, Y.L., LIU, L., DONG, J.Q., IDA, K., ITOH, K., SUN, A.P., CAO, J.Y., SHI, Z.B., WANG, Z.X., *et al.* 2016 Ion internal transport barrier in neutral beam heated plasmas on HL-2A. *Nucl. Fusion* **56** (5), 056003.
- ZHANG, B., GONG, X., QIAN, J., ZENG, L., XU, L.Q., DUAN, Y.M., ZHANG, J.Y., HU, Y.C., JIA, T.Q., LI, P., *et al.* 2022 Progress on physics understanding of improved confinement with fishbone instability at low q ($95 < 3.5$ operation regime in EAST. *Nucl. Fusion* **62** (12), 126064.
- ZHANG, X., WU, M.Q., LI, G., LI, G., TANG, T., YANG, Y., ZHONG, F.B., LONG, F.F., WU, M.F., ZHANG, T., *et al.* 2023 Investigation of key factors for ITB formation and maintenance in EAST high β discharges. *Phys. Lett. A* **462**, 128646.
- ZHANG, Y.Z. & MAHAJAN, S.M. 1992 Edge turbulence scaling with shear-flow. *Phys. Fluids B* **4** (6), 1385–1387.
- ZHU, X., ZENG, L., QIU, Z., HAO, B., SHEN, W., GU, X., WU, M., TANG, T., QIAN, J., LIU, H., *et al.* 2020 Dependence of fishbone cycle on energetic particle intensity in EAST low-magnetic-shear plasmas. *J. Plasma Phys.* **86** (6), 905860610.
- ZONCA, F., BURATTI, P., CARDINALI, A., CHEN, L., DONG, J.Q., LONG, Y.X., MILOVANOV, A.V., ROMANELLI, F., SMEULDERS, P., WANG, L., *et al.* 2007 Electron fishbones: theory and experimental evidence. *Nucl. Fusion* **47** (11), 1588–1597.